Solar Cells Based on Inks of n-Type Colloidal Quantum Dots

Zhijun Ning,[†,§] Haopeng Dong,[†,‡,§] Qiong Zhang,[†] Oleksandr Voznyy,[†] and Edward H. Sargent[*,†]

[†]Department of Electrical and Computer Engineering, University of Toronto, 10 King's College Road, Toronto, Ontario M5S 3G4, Canada and [‡]Key Lab of Organic Optoelectronics and Molecular Engineering of Ministry of Education, Department of Chemistry, Tsinghua University, Beijing, People's Republic of China. [§]Z. Ning and H. Dong contributed equally.

ABSTRACT New inorganic ligands including halide anions have significantly accelerated progress in colloidal quantum dot (CQD) photovoltaics in recent years. All such device reports to date have relied on halide treatment during solid-state ligand exchanges or on co-treatment of long-aliphatic-ligand-capped nanoparticles in the solution phase. Here we report solar cells based on a colloidal quantum dot ink that is capped using halide-based ligands alone. By judicious choice of solvents and ligands, we developed a CQD ink from which a homogeneous and thick colloidal quantum dot solid is applied in a single step. The resultant films display an n-type character, making it suitable as a key component in a solar-converting device. We demonstrate two types of quantum junction devices that exploit these iodide-ligand-based inks. We achieve solar power conversion efficiencies of 6% using this class of colloids.

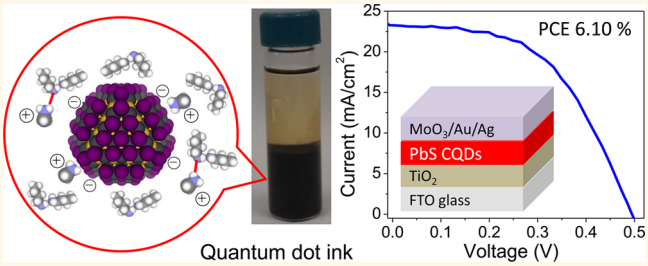

KEYWORDS: nanocrystals · solar cells · halide ligands · photodiode · n-type

Colloidal quantum dots (CQDs) have generated great interest worldwide for their promising applications in optoelectronic devices including light-emitting diodes,[1−3] photodetectors,[4,5] lasers,[6] solar concentrators,[7] and solar cells.[8−14] Their solution processability enables convenient manufacturing and prospectively lower cost compared to conventional single-crystalline solar cells.[15] Quantum-size tuning of the nanoparticles' band gap enables the realization of tandem solar cells based on a single materials system, an approach that raises the asymptote on solar power conversion efficiency beyond the Shockley−Quiesser limit.[16,17]

Recently, the efficiency of CQD solar cells has improved rapidly, with much progress enabled by both new device architectures, such as the quantum junction device, and the realization of improved quantum dot solids, including n-type CQD solids.[18−23]

All record-setting CQD solar cell performance results to date have relied on a solid-state ligand exchange,[18−23] wherein the long aliphatic ligands used in quantum dot synthesis are displaced on the processing substrate. Spin-coating and layer-by-layer exchange lead to vast material waste: typically only 1−10% of the consumed quantum dots are incorporated into the final film.

Recently, progress has been reported toward quantum dots that can instead be deposited directly onto a substrate, forming the final film in a single convenient and waste-free step.[24−27] The low performance of these devices was ascribed to reliance on a highly polar solvent, which, while it did provide the needed electrostatic stabilization using short ligands, also led to loss of halide surface anions crucial to efficient nanoparticle surface passivation.

In this work, we focus instead on producing a colloid that can be applied directly to process photovoltaic-quality films and that improves their performance considerably over all prior reports. We were inspired by two significant recent advances. In the first, Talapin and colleagues have realized nanoparticles passivated using inorganic metal chalcogenide ligands (MCCs),[28−30] suggesting that inorganic anions can be sufficient to confer colloidal stability. In parallel, we have shown[31−34] that halide passivation, applied in the solid state or the solution phase or both, can benefit solar cell performance by removing unwanted deep electronic trap

* Address correspondence to ted.sargent@utoronto.ca.

Received for review July 1, 2014 and accepted September 16, 2014.

Published online September 16, 2014
10.1021/nn503569p

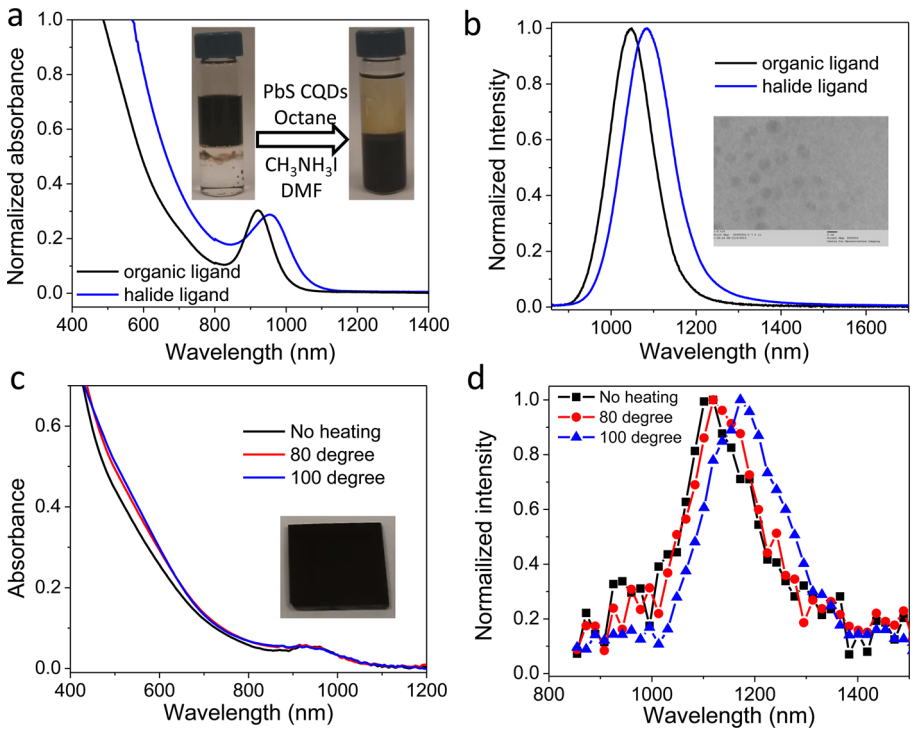

Figure 1. Absorption and emission spectra of CQDs in solution and film. (a) Absorption spectra of CQDs before and after iodide ligand exchange. A clear exciton peak is observed, indicating that quantum confinement was preserved. The inset images depict the two-phase ligand exchange process. Upon the completion of the ligand exchange, CQDs had transferred from the top octane phase to the bottom dimethylformamide (DMF) phase. (b) Photoluminescence (PL) spectra of CQDs before and after halide ligand exchange. The retention of the defined PL spectral feature confirms that quantum confinement was retained following inorganic ligand exchange. Inset is the TEM image of the CQDs after ligand exchange (scale bar 5 nm). (c) Absorption spectra of films before and after annealing. The exciton peak is retained even when the film is annealed at 100 °C. (d) Photoluminescence spectra of CQD films before and after annealing. The photoluminescence peak red-shifts with increasing annealing temperature but retains its defined character.

states. Recently, based on solution-phase iodide treatment and a layer-by-layer film-forming process, air stable n-type CQD films were reported.[23]

We took the view that if a complete halide-based ligand exchange can be made in the solution phase, a number of advantages would be provided. The nanoparticles would be well-passivated and well-protected from oxygen attack.[23] This could enable the first n-type quantum dot inks to be reported. The resultant inks would allow direct processing of a photovoltaic-quality CQD solid in a single step, overcoming the limitations and wastefulness of the legacy layer-by-layer approach.

RESULTS AND DISCUSSION

We synthesized PbS CQDs using lead(II) oleate with bis(trimethylsilyl) sulfide.[23] Prior to ligand exchange, the CQDs were dispersed in octane, and iodide salts (both CH_3NH_3I and NaI worked well) were dissolved in dimethylformamide (DMF) (γ-butyrolactone also worked well). We mixed these two phases vigorously and then kept them static until the phases became well-separated (inset of Figure 1a). After removing the top octane solution, we washed the CQDs in a polar solvent to remove the organic residue. We precipitated the CQDs *via* the addition of toluene and redispersed in butylamine (γ-butyrolactone also worked well) for film

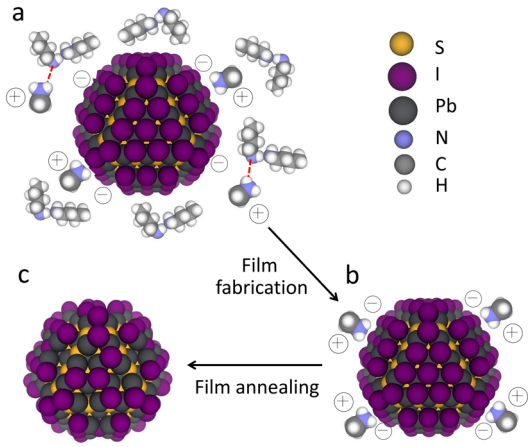

Figure 2. Schematic of surface ion distribution in quantum dot inks and films. (a) As-prepared CQDs after iodide ligand exchange in butylamine. Iodide anions bind to lead atoms on the CQD surface and are covered by methylammonium countercations. Methylammonium can desorb from the surface, stabilized by hydrogen bonds (red line) to butylamine. (b) As-prepared CQD films. The CQD surface is covered by counterions, maintaining charge neutrality. (c) CQD film after annealing. The ion pairs are eliminated, but the majority of iodide ligands remain on the CQD surface, providing passivation and charge-neutral stoichiometry.

fabrication. A schematic of iodide-capped CQDs in solution is presented in Figure 2. In addition to iodide

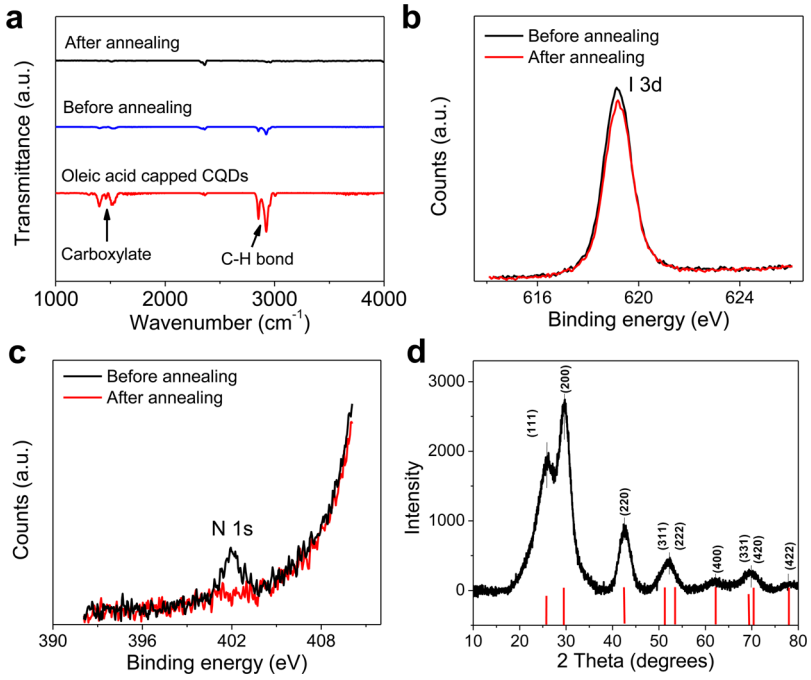

Figure 3. Characterization of films prepared from CQD ink. (a) Fourier transform infrared spectroscopy of CQD films with organic or halide ligands. Before annealing, a C−H stretching peak can be observed. However, after annealing, no C−H stretching peak was discernible following the halide ligand exchange. (b) X-ray photoelectron spectroscopy (XPS) measurement of the iodide 3d peak. The peak at 619.4 eV indicates lead-bound iodide, consistent with iodide ligands bonded to the CQD surface. After annealing, the iodide amount is reduced. (c) XPS measurement of the N 1s peak. After annealing, the N 1s peak at 401.9 eV disappeared, confirming that the organic residue was eliminated. (d) X-ray diffraction of the inorganic CQD ink confirms the presence of characteristic lead sulfide crystal peaks.

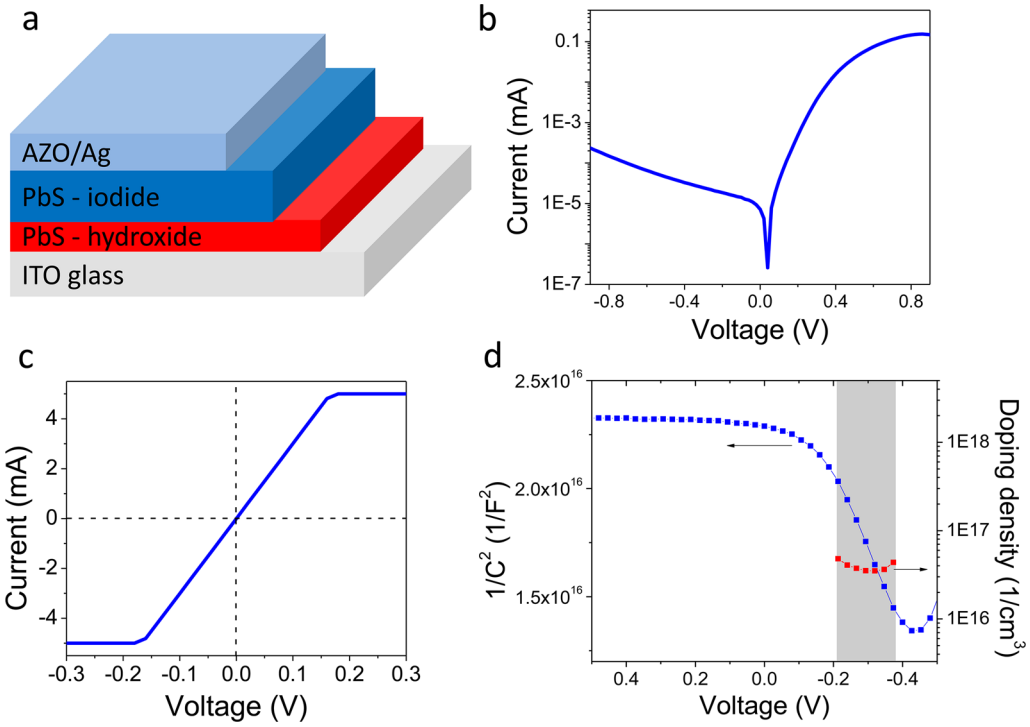

Figure 4. Electronic materials behavior of inorganic CQD ink-based films. (a) Quantum junction device structure: the n-type film employed the CQD ink, and the p-type layer was prepared using hydroxide in solid-state ligand exchange. (b) Dark current−voltage curve of the device, showing good rectification. (c) Dark current−voltage of the device without bottom p-type CQD layer (the highest current of 5 mA is limited by the ammeter). No rectification of the device was seen, consistent with the lack of junction with the aluminum-doped zinc oxide (AZO), thus the need for both p- and n-type quantum dots to form the rectifying junction. (d) Capacitance−voltage curve of the device. The calculated electron doping density of the film is ~3 × 10^{16} cm^{-3}, similar to the iodide ligand film that was prepared by solid-state ligand exchange.

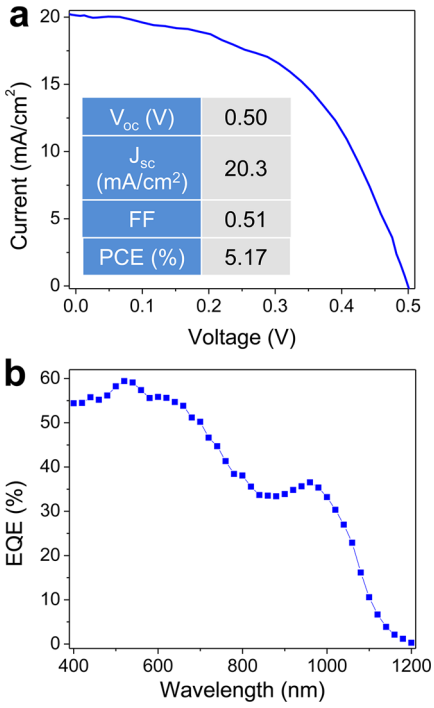

Figure 5. Photovoltaic device performance of quantum junction devices employing inorganic CQD inks. (a) Current–voltage curve of the quantum junction device under AM1.5 illumination. An overall power conversion efficiency of 5.17% was achieved. (b) External quantum efficiency (EQE) curve of the quantum junction device. The shape of the curve is similar to that of prior quantum junction solar cells. The relatively high EQE value across the fully absorbed visible range is consistent with the junction residing at the interface between p-type and n-type CQDs.

ligands required for CQD surface passivation, we propose that additional extra iodide ligands were bound to surface lead atoms and counterbalanced by methylammonium or sodium cations. These cations have a shallow electron affinity and do not affect the CQD passivation, as can be seen from density functional theory (DFT) results (Supporting Information).[35] The zeta potential of CQDs in γ-butyrolactone indicates a negatively charged CQD (−8.2 eV) (Supporting Information), consistent with a more labile positive counterion layer. Although the polarity of butylamine is relatively low, its basic character enables it to remove methylammonium ions partially from the CQD surface (Figure 2a), stabilizing them in solution *via* hydrogen bonds (the calculated binding energy of methylammonium to CQD is 18 kcal/mol after inclusion of solvent effects). The existence of unbalanced iodide ions on the CQD surface gives rise to an electrostatic repulsive interaction between CQDs, thereby stabilizing the colloidal nanoparticles in solution.[36] The adsorption of ions is critical to keep the colloidal character of the CQDs: if we wash the CQDs one more time with DMF and toluene to remove surface ions, then they can no longer be redispersed in butylamine.

Absorption and emission spectra of exchanged CQDs in solution (Figure 1a,b) reveal a slightly red-shifted exciton peak, consistent with a decrease in confinement due to a shallower iodide HOMO compared to the original oleate ligands (Supporting Information). The photoluminescence peak retains its intensity and narrowness and is similarly shifted slightly to the red. Transmission electron microscopy (TEM) (Figure 1b) confirms that the nanoparticles remained distinct and well-dispersed in the final colloid. Both bromide and chloride ligands were also investigated in the ligand exchange, but neither enabled a stable colloid, consistent with the previous findings that the bonding of chloride and bromide is insufficiently strong.[23]

We then turned to the realization of CQD solids based on the halide-terminated quantum dot inks. We found that butylamine, with its low boiling temperature, facilitated the fabrication of homogeneous thick films. The resultant film absorption and emission spectra (Figure 1c,d) exhibit peaks at locations identical to those in solution, confirming that quantum confinement was retained.

To remove solvent residues, we annealed the films at 100 °C (Figure 2b,c). Remarkably, no obvious shift of the absorption peak was observed even with annealing: the exciton peak remained sharp in both absorption and emission. Fourier transform infrared spectroscopy (FTIR) (Figure 3a) confirms that annealing was sufficient to remove organic residue from the film and produce an all-inorganic quantum dot solid. X-ray photoelectron spectroscopy (XPS) shows the iodide signal at 619.4 eV, consistent with iodide bound to the CQD surface (Figure 3b).[21] The N 1s peak at 402 eV in nonannealed film indicates NH^{3+} species at a level of few tens of ions per CQD (Figure 3c). After annealing it was eliminated, indicating that annealing can effectively remove the counterions from the film. The iodide content in the film was reduced as well, suggesting that ammonium ligands desorb paired with iodide, thus maintaining the charge neutrality of CQDs (Figure 2c). Based on DFT simulation, the energy of ion pair desorption is 40 kcal/mol, consistent with mild heat being sufficient to remove ion pairs. The iodide to lead ratio in the final film is 0.65. The large amount of iodine remaining in the films is sufficient to maintain high-quality passivation. X-ray diffraction (XRD) (Figure 3d) shows the expected PbS crystal peaks in exchanged films.[37]

Recent reports indicate that the use of iodide treatments can bring n-type doping to CQD solids and even produce an air-stable n-type CQD film.[23,38] We investigated the net doping type of the iodide-capped CQD inks by deploying them in quantum junction solar cells (Figure 4a).[32] The bottom p-type layer is fabricated by strongly oxidizing these lower layers using tetramethylammonium hydroxide. The top half of the device was formed using the directly deposited CQD ink layer. We used ITO (indium doped tin oxide)-on-glass as the substrate and aluminum-doped zinc oxide (AZO) and silver as the top contact. The dark current–voltage

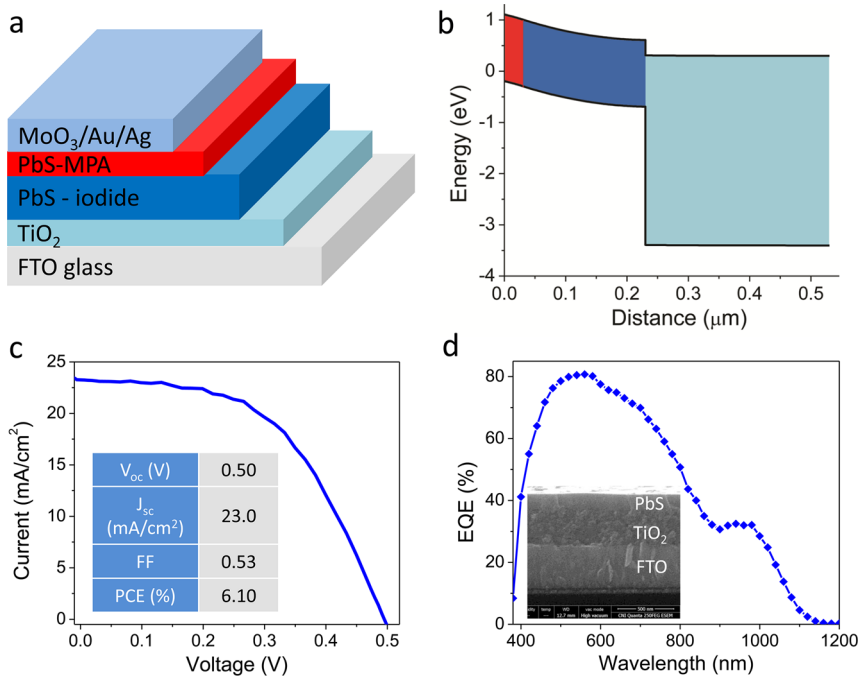

Figure 6. Photovoltaic device performance of inverted quantum junction devices employing inorganic CQD inks. (a) Diagram of device structure. The n-type layer was fabricated using the inorganic CQD ink, and the p-type layer on top was made by using mercaptopropionic acid (MPA) as ligand. (b) Simulated spatial band diagrams of the device operating at equilibrium, with modeling performed using SCAPS. In light of the measured n-type doping, the n-type CQD close to TiO_2 is predicted not to be fully depleted, which could lower the light-harvesting efficiency in the short-wavelength region. (c) Current–voltage curves of the device under AM1.5 illumination. Over 6% power conversion efficiency was achieved. (d) EQE spectrum of the inverted quantum junction device. The relatively low EQE value in the blue region is again consistent with the junction being located at the n- to p-type CQD interface. Inset is the scanning electron microscopy image of the CQD film cross-section on TiO_2 substrate (scale bar 500 nm).

characteristic (Figure 4b) reveals excellent rectification. We prepared control devices consisting of either (a) only the bottom p-type layer or (b) only the top halide layer and found that each failed to rectify (Figure 4c). This is consistent with the view that the strongly p-type bottom layer formed a junction with a top n-type layer. Because the bottom p-type layer is known to have high doping in the 10^{18} cm^{-3} range,[20] capacitance–voltage analysis of these junction devices allowed us to estimate the doping density of the top n-type ink-based film at $\sim 3 \times 10^{16}$ cm^{-3}.

We characterized the devices in air and found that their rectification and performance were retained compared to in-glovebox tests. The device performance of the solar cells under AM1.5 illumination is shown in Figure 5a. The short-circuit current and open-circuit voltage are 20 mA/cm^2 and 0.50 V, respectively. The slightly lower photocurrent compared to the best CQD devices is consistent with the known high defect level in the highly oxidized p-type layer.[32] The spectrally flat external quantum efficiency (Figure 5b) across the 400–650 nm range in which substantially all incident light is absorbed is again consistent with the establishment of the rectifying junction at the p-type to n-type CQD interface.[23]

In light of these indications of a high defect concentration in the p-type layer, we turned to an improved device, the inverted quantum junction (Figure 6a,b[39]), with the goal of combining a higher performance p-type film with our novel n-type layer.[23] CQD films were fabricated on a TiO_2 substrate using the n-type CQD ink, after which a thin mildly p-type MPA-treated CQD layer (~30 nm) was added, followed by a MoO_3/Au/Ag top contact. A cross-sectional scanning electron microscope (SEM) image (Figure 6d) reveals that the bottom ink-based layer was approximately 200 nm thick.

The measured current–voltage curve under AM1.5 illumination is shown in Figure 6c. Compared with conventional quantum junction devices, an improved short-circuit current of 23 mA/cm^2 is achieved, ascribed to the removal of the highly doped and defective p-type film. The power conversion efficiency exceeds 6%. The external quantum efficiency spectrum of the device is shown in Figure 6d. The low external quantum efficiency (EQE) value in the blue spectral region suggests that the n-type layer is slightly less than fully depleted.[23]

CONCLUSIONS

This study presented the first photovoltaic-quality n-type colloidal quantum dot ink. It also represents the first solution-phase inorganic-ligand-exchanged quantum dot solid to be featured in a solar cell.

The mechanism of colloidal stabilization using methylammonium iodide ligands was clarified using DFT simulations. The best devices realized so far using this new class of materials provided a 6% solar power conversion efficiency. The ink can be directly deposited in a single step, with no requirement of solid-state exchange, rendering it compatible with roll-to-roll processes such as screen printing, spray coating, and blade coating. The film provided an impressive stability at 100 °C and was successfully tested in air. The work proves that halide-ligand-based inks offer a promising further path to efficient, low-cost, and stable CQD solar cells.

During the time of preparation of this manuscript, the Wang, Kovalenko, and Talapin groups presented related solution-phase ligand exchanges; however, no CQDs films nor devices were reported.[40−42]

METHODS

Ligand Exchange and Film Fabrication. CQDs were synthesized using previously reported methods.[23] A 4 mL amount of CQDs dispersed in octane (10 mg/mL) was added to 3 mL of CH_3NH_3I dispersed in DMF (80 mg/mL). These were mixed vigorously for several minutes until the CQDs moved from the top octane solvent to the bottom DMF phase. The DMF solution was washed three times using octane. After precipitation of CQDs by the addition of toluene, the nanoparticles were dispersed in butylamine (200 mg/mL) for film fabrication. Films were prepared by spin-coating at a spin speed of 6000 rpm.

Solar Cell Fabrication. The p-type film in the quantum junction device was prepared by using tetramethylammonium hydroxide for ligand exchange, as reported previously.[32] On the top of the n-type CQD film, an aluminum-doped zinc oxide (30 nm) film was prepared by sputtering, followed by thermal deposition of silver (300 nm).[23] For inverted quantum junction solar cells, the bottom TiO_2 film is composed of two layers. The first layer is fabricated by atomic layer deposition (220 cycle, Cambridge Nanotech Savannah), and the second layer is prepared by DS18 paste (300 nm), as previously reported.[43] The top p-type layer is fabricated by MPA ligand exchange, also as previously reported.[23] The top contact MoO_3/Au/Ag layers are fabricated using the same processes reported in previous works.[33]

PCE Characterization. Current−voltage characteristics were measured using a Keithley 2400 source-meter. The solar cells were each tested in air. The solar spectrum at AM1.5 was simulated to within class A specifications (less than 25% spectral mismatch) with a Xe lamp and filters (Solar Light Company Inc.) with measured intensity at 100.6 mW/cm^2. The source intensity was measured using a Melles-Griot broadband power meter and a Thorlabs broadband power meter through a circular 0.049 cm^2 aperture at the position of the device and confirmed with a calibrated reference solar cell (Newport, Inc.). The accuracy of the power measurement was estimated to be ±5%.

Characterization. For FTIR measurement, the sample fabrication process is the same as that used for solar cell measurement. The reflection model was used, and the curve was adjusted by using the baseline correction method. The equipment model is Bruker Tensor 27. Capacitance−voltage measurements were performed directly on the photovoltaic devices using an Agilent 4284A LCR meter at a frequency of 1 kHz. The scanning speed is 0.02 V/s.

Conflict of Interest: The authors declare no competing financial interest.

Acknowledgment. This publication is based in part on work supported by Award KUS-11-009-21, from King Abdullah University of Science and Technology (KAUST), by the Ontario Research Fund - Research Excellence Program, and by the Natural Sciences and Engineering Research Council (NSERC) of Canada. H.D. would like to acknowledge a scholarship from the China Scholarship Council (CSC). Computations were performed on the GPC supercomputer at the SciNet HPC Consortium. SciNet is funded by the Canada Foundation for Innovation under the auspices of Compute Canada; the Government of Ontario; Ontario Research Fund - Research Excellence; and the University of Toronto. We thank Angstrom Engineering, Inc. and Innovative Technology, Inc. for useful discussions regarding material deposition methods and control of the glovebox environment, respectively. The authors thank L. Levina for CQD synthesis, L. Rollny for the zeta potential measurements, F. Fan for TEM measurements, J. McDowell for the XRD measurements, H. F. Movahed for SCAPS simulations, and E. Palmiano, R. Wolowiec, and D. Kopilovic for their help during the course of these studies.

Supporting Information Available: Density of states; zeta potential of solution-exchanged PbS CQDs. This material is available free of charge *via* the Internet at http://pubs.acs.org.

Note Added after ASAP Publication: After this paper was published ASAP on September 22, 2014, a correction was made to Figure 3c. The corrected version was reposted September 26, 2014.

REFERENCES AND NOTES

1. Wood, V. M.; Panzer, J.; Chen, J.; Bradley, M. S.; Halpert, J. E.; Bawendi, M. G.; Bulović, V. Inkjet-Printed Quantum Dot-Polymer Composites for Full-Color AC-Driven Displays. *Adv. Mater.* **2009**, *21*, 2151–2155.
2. Sun, Q. J.; Wang, Y. A.; Li, L. S.; Wang, D. Y.; Zhu, T.; Yang, C. H.; Li, Y. F. Bright, Multicoloured Light-Emitting Diodes Based on Quantum Dots. *Nat. Photonics* **2007**, *1*, 717–722.
3. Jeonghun, K.; Wan, K. B.; Lee, D. G.; Park, I.; Lim, J.; Park, M.; Cho, H.; Woo, H.; Yoon, D. Y.; Char, K.; *et al*. Bright and Efficient Full-Color Colloidal Quantum Dot Light-Emitting Diodes Using an Inverted Device Structure. *Nano Lett.* **2012**, *12*, 2362–2366.
4. Konstantatos, G.; Howard, I.; Fischer, A.; Hoogland, S.; Clifford, J.; Klem, E.; Levina, L.; Sargent, E. H. Ultrasensitive Solution-Cast Quantum Dot Photodetectors. *Nature* **2006**, *442*, 180–183.
5. Lee, J.-S.; Maksym, V. K.; Huang, J.; Chung, D. S.; Dmitri, V. T. Band-Like Transport, High Electron Mobility and High Photoconductivity in All-Inorganic Nanocrystal Arrays. *Nat. Nanotechnol.* **2011**, *6*, 348–352.
6. Hoogland, S.; Sukhovatkin, V.; Howard, I.; Cauchi, S.; Levina, L.; Sargent, E. H. A Solution-Processed 1.53 um Quantum Dot Laser with Temperature-Invariant Emission Wavelength. *Opt. Express* **2006**, *14*, 3273–3281.
7. Meinardi, F.; Colombo, A.; Velizhanin, K. A.; Simonutti, R.; Lorenzon, M.; Beverina, L.; Viswanatha, R.; Klimov, V. I.; Brovelli, S. Large-Area Luminescent Solar Concentrators Based on 'Stokes-Shift-Engineered' Nanocrystals in a Mass-Polymerized PMMA Matrix. *Nat. Photonics* **2014**, *8*, 392–399.
8. Oh, S. J.; Berry, N. E.; Choi, J.-H.; Gaulding, E. A.; Paik, T.; Hong, S.-H.; Murray, C. B.; Kagan, C. R. Stoichiometric Control of Lead Chalcogenide Nanocrystal Solids to Enhance Their Electronic and Optoelectronic Device Performance. *ACS Nano* **2013**, *7*, 2413–2421.
9. Beard, M. C.; Luther, J. M.; Semonin, O. E.; Nozik, A. J. Third Generation Photovoltaics Based on Multiple Exciton Generation in Quantum Confined Semiconductors. *Acc. Chem. Res.* **2013**, *46*, 1252–1260.
10. Brown, P. R.; Lunt, R. R.; Zhao, N.; Osedach, T. P.; Wanger, D. D.; Chang, L.-Y.; Bawendi, M. G.; Bulović, V. Improved Current Extraction from ZnO/PbS Quantum Dot

Heterojunction Photovoltaics Using a MoO_3 Interfacial Layer. *Nano Lett.* **2011**, *11*, 2955–2961.
11. Ma, W.; Swisher, S. L.; Ewers, T.; Engel, J.; Ferry, V. E.; Atwater, H. A.; Alivisatos, A. P. Photovoltaic Performance of Ultrasmall PbSe Quantum Dots. *ACS Nano* **2011**, *5*, 8140–8147.
12. Chuang, C.-H. M.; Brown, P. R.; Bulović, V.; Bawendi, M. G. Improved Performance and Stability in Quantum Dot Solar Cells through Band Alignment Engineering. *Nat. Mater.* **2014**, *13*, 796–801.
13. Ning, Z.; Yuan, C.; Tian, H.; Hedström, P.; Sun, L.; Ågren, H. Quantum Rod-Sensitized Solar Cells. *ChemSusChem* **2011**, *4*, 1741–1744.
14. Lan, X.; Bai, J.; Masala, S.; Thon, S. M.; Ren, Y.; Kramer, I. J.; Hoogland, S.; Simchi, A.; Koleilat, G. I.; Paz-Soldan, D.; *et al*. Self-Assembled, Nanowire Network Electrodes for Depleted Bulk Heterojunction Solar Cells. *Adv. Mater.* **2013**, *25*, 1769–1773.
15. Talapin, D. V.; Murray, C. B. PbSe Nanocrystals Solids for *n*- and *p*-Channel Thin Film Field-Effect Transistors. *Science* **2005**, *310*, 86–89.
16. Wang, X.; Koleilat, G.; Tang, J.; Liu, H.; Kramer, I. J.; Debnath, R.; Brzozowski, L.; Barkhouse, D. A. R.; Levina, L.; Hoogland, S.; *et al*. Tandem Colloidal Quantum Dot Solar Cells Employing a Graded Recombination Layer. *Nat. Photonics* **2011**, *5*, 480–484.
17. Choi, J. J.; Wenger, W. N.; Hoffman, R. S.; Lim, Y.-F.; Luria, J.; Jasieniak, J.; Marohn, J. A.; Hanrath, T. Solution-Processed Nanocrystal Quantum Dot Tandem Solar Cells. *Adv. Mater.* **2011**, *23*, 3144–3148.
18. Zhitomirsky, D.; Voznyy, O.; Levina, L.; Hoogland, S.; Kemp, K. W.; Ip, A. H.; Thon, S. M.; Sargent, E. H. Engineering Colloidal Quantum Dot Solids within and beyond the Mobility-Invariant Regime. *Nat. Commun.* **2014**, *5*, 3803.
19. Ning, Z.; Zhitomirsky, D.; Adinolfi, V.; Sutherland, B.; Xu, J.; Voznyy, O.; Maraghechi, P.; Lan, X.; Hoogland, S.; Ren, Y.; Sargent, E. H. Graded Doping for Enhanced Colloidal Quantum Dot Photovoltaics. *Adv. Mater.* **2013**, *25*, 1719–1723.
20. Tang, J.; Liu, H.; Zhitomirsky, D.; Hoogland, S.; Wang, X.; Furukawa, M.; Levina, L.; Sargent, E. H. Quantum Junction Solar Cells. *Nano Lett.* **2012**, *12*, 4889–4894.
21. Zhitomirsky, D.; Furukawa, M.; Tang, J.; Stadler, P.; Hoogland, S.; Voznyy, O.; Liu, H.; Sargent, E. H. N-Type Colloidal-Quantum-Dot Solids for Photovoltaics. *Adv. Mater.* **2012**, *24*, 6181–6185.
22. Voznyy, O.; Zhitomirsky, D.; Stadler, P.; Ning, Z.; Hoogland, S.; Sargent, E. H. A Charge-Orbital Balance Picture of Doping in Colloidal Quantum Dot Solids. *ACS Nano* **2012**, *6*, 8448–8455.
23. Ning, Z.; Voznyy, O.; Pan, J.; Hoogland, S.; Adinolfi, V.; Xu, J.; Li, M.; Kirmani, A. R.; Sun, J.; Minor, J.; *et al*. Air-Stable n-Type Colloidal Quantum Dot Solids. *Nat. Mater.* **2014**, *13*, 822–828.
24. Fischer, A.; Rollny, L.; Pan, J.; Carey, G. H.; Thon, S. M.; Hoogland, S.; Voznyy, O.; Zhitomirsky, D.; Kim, J. Y.; Bakr, O. M.; *et al*. Directly Deposited Quantum Dot Solids Using a Colloidally Stable Nanoparticle Ink. *Adv. Mater.* **2013**, *25*, 5742–5749.
25. Kirmani, A. R.; Carey, G. H.; Abdelsamie, M.; Yan, B.; Cha, D.; Rollny, L. R.; Cui, X.; Sargent, E. H.; Amassian, A. Effect of Solvent Environment on Colloidal-Quantum-Dot Solar-Cell Manufacturability and Performance. *Adv. Mater.* **2014**, *26*, 4717–4723.
26. Giansante, C.; Carbone, L.; Giannini, C.; Altamura, D.; Ameer, Z.; Maruccio, G.; Loiudice, A.; Belviso, M. R.; Cozzoli, P. D.; Rizzo, A.; *et al*. Colloidal Arenethiolate-Capped PbS Quantum Dots: Optoelectronic Properties, Self-Assembly, and Application in Solution-Cast Photovoltaics. *J. Phys. Chem. C* **2013**, *117*, 13305–13317.
27. Norman, Z. M.; Anderson, N. C.; Owen, J. S. Electrical Transport and Grain Growth in Solution-Cast, Chloride-Terminated Cadmium Selenide Nanocrystal Thin Films. *ACS Nano* **2014**, *8*, 7513–7521.
28. Kovalenko, M. V.; Scheele, M.; Talapin, D. V. Colloidal Nanocrystals with Molecular Metal Chalcogenide Surface Ligands. *Science* **2009**, *324*, 1417–1420.
29. Kovalenko, M. V.; Bodnarchuk, M. I.; Zaumseil, J.; Lee, J.-S.; Talapin, D. V. Expanding the Chemical Versatility of Colloidal Nanocrystals Capped with Molecular Metal halcogenide Ligands. *J. Am. Soc. Chem.* **2010**, *132*, 10085–10092.
30. Talapin, D. V.; Lee, J.-S.; Kovalenko, M. V.; Shevchenko, E. V. Prospects of Colloidal Nanocrystals for Electronic and Optoelectronic Applications. *Chem. Rev.* **2010**, *110*, 389–458.
31. Tang, J.; Kemp, K. W.; Hoogland, S.; Jeong, K. S.; Liu, H.; Levina, L.; Furukawa, M.; Wang, X.; Debnath, R.; Cha, D.; *et al*. Colloidal-Quantum-Dot Photovoltaics Using Atomic-Ligand Passivation. *Nat. Mater.* **2011**, *10*, 765–771.
32. Ning, Z.; Ren, Y.; Hoogland, S.; Voznyy, O.; Levina, L.; Stadler, P.; Lan, X.; Zhitomirsky, D.; Sargent, E. H. All-Inorganic Colloidal Quantum Dot Photovoltaics Employing Solution-Phase Halide Passivation. *Adv. Mater.* **2012**, *24*, 6295–6299.
33. Ip, A. H.; Thon, S. M.; Hoogland, S.; Voznyy, O.; Zhitomirsky, D.; Debnath, R.; Levina, L.; Rollny, L. R.; Carey, G. H.; Fischer, A.; *et al*. Hybrid Passivated Colloidal Quantum Dot Solids. *Nat. Nanotechnol.* **2012**, *7*, 577–582.
34. Wang, H.; Kubo, T.; Nakazaki, J.; Kinoshita, T.; Segawa, H. PbS-Quantum-Dot-Based Heterojunction Solar Cells Utilizing ZnO Nanowires for High External Quantum Efficiency in the Near-Infrared Region. *J. Phys. Chem. Lett.* **2013**, *4*, 2455–2460.
35. Vande Vondele, J.; Krack, M.; Mohamedb, F.; Parrinellob, M.; Chassaingc, T.; Hutterc, J. Quickstep: Fast and Accurate Density Functional Calculations Using a Mixed Gaussian and Plane Waves Approach. *Comput. Phys. Commun.* **2005**, *167*, 103–128.
36. Reichardt, C. Solvatochromic Dyes as Solvent Polarity Indicators. *Chem. Rev.* **1994**, *94*, 2319–2358.
37. Tang, J.; Brzozowski, L.; Barkhouse, D. A. R.; Wang, X.; Debnath, R.; Wolowiec, R.; Palmiano, E.; Levina, L.; Pattantyus-Abraham, A. G.; Jamakosmanovic, D.; *et al*. Quantum Dot Photovoltaics in the Extreme Quantum Confinement Regime: The Surface-Chemical Origins of Exceptional Air- and Light-Stability. *ACS Nano* **2010**, *4*, 869–878.
38. Jeong, K. S.; Deng, Z.; Keuleyan, S.; Liu, H.; Guyot-Sionnest, P. Air-Stable n-Doped Colloidal HgS Quantum Dots. *J. Phys. Chem. Lett.* **2014**, *5*, 1139–1143.
39. Burgelman, M.; Nollet, P.; Degrave, S. Modelling Polycrystalline Semiconductor Solar Cells. *Thin Solid Films* **2000**, *361−362*, 527–532.
40. Niu, G.; Wang, L.; Gao, R.; Li, W.; Guo, X.; Dong, H.; Qiu, Y. Inorganic Halogen Ligands in Quantum Dots: I^-, Br^-, Cl^- and Film Fabrication through Electrophoretic Deposition. *Phys. Chem. Chem. Phys.* **2013**, *15*, 19595–19600.
41. Zhang, H.; Jang, J.; Liu, W.; Talapin, D. V. Colloidal Nanocrystals with Inorganic Halide, Pseudohalide, and Halometallate Ligands. *ACS Nano* **2014**, *8*, 7359–7369.
42. Dirin, D. N.; Dreyfuss, S.; Bodnarchuk, M. I.; Nedelcu, G.; Papagiorgis, P.; Itskos, G.; Kovalenko, M. V. Lead Halide Perovskites and Other Metal Halide Complexes as Inorganic Capping Ligands for Colloidal Nanocrystals. *J. Am. Chem. Soc.* **2014**, *136*, 6550–6553.
43. Burschka, J.; Pellet, N.; Moon, S.-J.; Humphry-Baker, R.; Gao, P.; Nazeeruddin, M. K.; Grätzel, M. Sequential Deposition as a Route to High-Performance Perovskite-Sensitized Solar Cells. *Nature* **2013**, *499*, 316–319.